PROCEEDINGS OF SCIENCE

# 21cm Forest with the SKA

**Benedetta Ciardi**
*Max Planck Institute for Astrophysics, Garching, Germany*
*E-mail:* ciardi at mpa-garching.mpg.de

**Susumu Inoue**
*Institute for Cosmic Ray Research, University of Tokyo, Tokyo, Japan*
*E-mail:* sinoue at icrr.u-tokyo.ac.jp

**Katherine J. Mack**
*University of Melbourne, Melbourne, Australia*
*E-mail:* kmack at unimelb.edu.au

**Yidong Xu**
*National Astronomical Observatories, Chinese Academy of Sciences, Beijing, China*
*E-mail:* xuyd at nao.cas.cn

**Gianni Bernardi***
*SKA SA, Cape Town, South Africa*
*Rhodes University, Grahamstown, South Africa*
*E-mail:* giannibernardi at ska.ac.za

An alternative to both the tomography technique and the power spectrum approach is to search for the 21cm forest, that is the 21cm absorption features against high-$z$ radio loud sources caused by the intervening cold neutral intergalactic medum (IGM) and collapsed structures. Although the existence of high-$z$ radio loud sources has not been confirmed yet, SKA-low would be the instrument of choice to find such sources as they are expected to have spectra steeper than their lower-$z$ counterparts. Since the strongest absorption features arise from small scale structures (few tens of physical kpc, or even lower), the 21cm forest can probe the HI density power spectrum on small scales not amenable to measurements by any other means. Also, it can be a unique probe of the heating process and the thermal history of the early universe, as the signal is strongly dependent on the IGM temperature. Here we show what SKA1-low could do in terms of detecting the 21cm forest in the redshift range $z \sim 7.5 - 15$.

*Advancing Astrophysics with the Square Kilometre Array*
*June 8-13, 2014*
*Giardini Naxos, Italy*

*Speaker.

 

PoS(AASKA14)006

## 1. Introduction

An alternative to both the tomography technique and the power spectrum approach is to search for the 21cm forest, that is the 21cm absorption features against high-$z$ radio loud sources caused by the intervening cold neutral IGM and collapsed structures (e.g. Carilli, Gnedin & Owen 2002; Furlanetto & Loeb 2002; Furlanetto 2006; Carilli et al. 2007; Xu et al. 2009; Xu, Ferrara & Chen 2011; Mack & Wyithe 2012; Ciardi et al. 2013; Ewall-Wice et al. 2014). In fact the 21cm forest is more than a complement to tomography or power spectrum analysis. Since the strongest absorption features arise from small scale structures, the 21cm forest can probe the HI density power spectrum on small scales not amenable to measurements by any other means (e.g. Shimabukuro et al. 2014). Also, it can be a unique probe of the heating process and the thermal history of the early universe, as the signal is strongly dependent on the IGM temperature.

The photons emitted by a radio loud source at redshift $z_s$ with frequencies $\nu > \nu_{21\rm cm}$, will be removed from the source spectrum with a probability $1-e^{-\tau_{21\rm cm}}$, absorbed by the neutral hydrogen present along the line of sight (LOS) at redshift $z = \nu_{21\rm cm}/\nu(1+z_s)-1$. The optical depth $\tau_{21\rm cm}$ can be written as (e.g. Madau, Meiksin & Rees 1997; Furlanetto, Oh & Briggs 2006):

$$\tau_{21\rm cm}(z) = \frac{3}{32\pi}\frac{h_p c^3 A_{21\rm cm}}{k_B \nu_{21\rm cm}^2}\frac{x_{\rm HI} n_{\rm H}}{T_s(1+z)(dv_\parallel/dr_\parallel)}, \tag{1.1}$$

where $n_{\rm H}$ is the H number density, $x_{\rm HI}$ is the mean neutral hydrogen fraction, $T_s$ is the gas spin temperature (which quantifies the relative population of the two levels of the $^2S_{1/2}$ transition), $A_{21\rm cm} = 2.85\times10^{-15}$ s$^{-1}$ is the Einstein coefficient of the transition and $dv_\parallel/dr_\parallel$ is the gradient of the proper velocity along the LOS (in km s$^{-1}$), which takes into account also the contribution of the gas peculiar velocity. The other symbols appearing in the equation above have the standard meaning adopted in the literature.

Analogously to the case of the Ly-$\alpha$ forest, this could result in an average suppression of the source flux (produced by diffuse neutral hydrogen), as well as in a series of isolated absorption lines (produced by overdense clumps of neutral hydrogen), with the strongest absorption associated with high density, neutral and cold patches of gas. This suggests that the absorption features due to collapsed structures with no or very small star formation (to maximize the amount of HI available for absorption), such as minihalos or dwarf galaxies (Furlanetto & Loeb 2002; Meiksin 2011; Xu, Ferrara & Chen 2011) would be easier to detect than those due to the diffuse neutral IGM. However, this does strongly depend on the feedback effects acting on such objects. Because of the large uncertainties in the nature and intensity of high-$z$ feedback effects (for a review see Ciardi & Ferrara 2005 and its updated version arXiv:astro-ph/0409018), it is not straightforward to estimate the relative importance of the absorption signals from the diffuse IGM and from collapsed objects.

While gas which has been (even only partially) ionized has a temperature of $\sim 10^4$ K, gas which has not been reached by ionizing photons has a temperature which can be even lower that of the CMB. This neutral gas can be heated by Ly-$\alpha$ or X-ray photons, thus reducing the optical depth to 21cm. While Ly-$\alpha$ heating is not extremely efficient, heating due to X-ray photons could easily suppress the otherwise present absorption features (e.g. Mack & Wyithe 2012; Ciardi et al. 2013). This seems to suggest that with observations of the 21cm forest it would be possible to discriminate between different IGM reheating histories, in particular if a high energy component in the ionising spectrum were present (Ewall-Wice et al. 2013).

## 2. Observed spectra

In this Section we describe the process used to simulate an observed spectrum. The simulated absorption spectrum, $S_{\rm abs}$, is calculated from a full 3D radiative transfer simulation of IGM reionization which resolves scales of $\sim 1$ kHz (corresponding to $\sim$50 kpc comoving; Ciardi et al. 2012; Ciardi et al. 2013). In the simulation used here, the contribution to ionization and heating from x-rays and/or Ly-$\alpha$ photons is not included (although see Ciardi et al. 2013 for examples of spectra which include such effects), i.e. the gas which is not reached by UV ionizing photons remains cold.

The instrumental effects are estimated using the pipeline of the LOFAR telescope. More specifically, the equation giving the observed visibilities is:

$$V_\nu(\mathbf{u}) = \sum_i^{N_{sources}} I_\nu(\mathbf{s}) e^{-2\pi i \mathbf{u}\cdot\mathbf{s}} + n_s, \tag{2.1}$$

where $\mathbf{u} = (u,v,w)$ are the coordinates of a given baseline at a certain time $t$, $I_\nu$ is the observed source intensity, $\mathbf{s} = (l,m,n)$ is a vector representing the direction cosines for a given source direction and $n_s$ represents additive noise. The noise is given by the radiometer equation:

$$n_s = \frac{1}{\eta_s}\frac{SEFD}{\sqrt{2t_{\rm int}\Delta\nu}}, \tag{2.2}$$

where $\eta_s$ is the system efficiency, $\Delta\nu$ is the bandwidth and $t_{int}$ is the integration time. Because of our experience with the LOFAR telescope, we will make predictions based on its characteristics, and we will then scale the noise to match the one expected from SKA. We thus assume that $\eta_s = 0.5$ and $N_{st} = 48$. The system equivalent flux density is given by:

$$SEFD = \frac{2\kappa_B T_{\rm sys}}{N_{\rm dip}\eta_\alpha A_{\rm eff}}, \tag{2.3}$$

where $\kappa_B$ is Boltzmann's constant, $A_{\rm eff} = min(\frac{\lambda 2}{3}, 1.5626)$ is the effective area of each dipole in the dense and sparse array regimes respectively, $N_{\rm dip}$ is the number of dipoles per station (24 tiles times 16 dipoles per tile for a LOFAR core station) and $\eta_\alpha$ is the dipole efficiency which we assume to be 1. The system noise $T_{\rm sys}$ has two contributions: *(i)* from the electronics and *(ii)* from the sky. We assume that the sky has a spectral index of -2.55, obtaining $T_{\rm sys} = [140 + 60(\nu/150\,{\rm MHz})^{-2.55}]$ K. The complete Fourier plane sampling can be done by evaluating the above equation for every set of baseline coordinates. The predicted visibilities are then gridded and transformed via inverse Fourier transforms in order to obtain the dirty images. For the purpose of the 21 cm forest, fine spectral resolution ($\sim$1 kHz, see later for further discussion) is needed, which means that the spectra need to be predicted for a large number of channels ($\sim 10000$). After assembling the full image cube, the LOS spectrum is extracted. In principle, the effect of the Point Spread Function (PSF) side lobes running through the source of interest can be taken into account by including more sources at different positions, with or without absorption features. Here, we have ignored the effect of side lobe noise. In fact, as the SKA will have a very dense uv coverage and the expected 21cm absorption lines will be narrower than a few tens of kHz, we expect the side lobe noise to play a marginal role.

Figure 1 shows the 21cm absorption spectrum due to the diffuse IGM along a random LOS for a bright radio source at $z = 10$ (i.e. $\nu \sim 129$ MHz). For an easy comparison to existing work

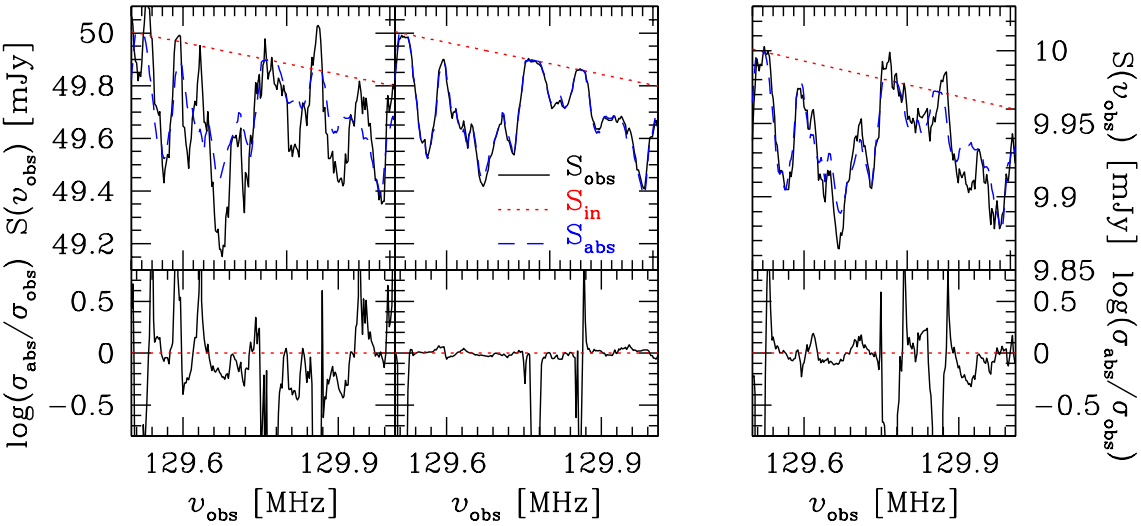


**Figure 1:** *Upper panels:* Spectrum of a radio source positioned at $z = 10$ ($\nu \sim 129$ MHz), with a power-law index $\alpha = 1.05$ and a flux density $J = 50$ mJy (left hand panels) and 10 mJy (right hand panel). The red dotted lines refer to the instrinsic spectrum of the radio source, $S_{\rm in}$; the blue dashed lines to the simulated spectrum for 21cm absorption, $S_{\rm abs}$ (in a universe where neutral regions remain cold); and the black solid lines to the spectrum for 21cm absorption as it would be seen with an observation time $t_{\rm int} = 1000$ h and a frequency resolution $\Delta\nu = 10$ kHz. The first panel to the left corresponds to a case with the LOFAR noise, while the other two panels have 1/10th of the LOFAR noise, roughly expected for SKA1-low. *Lower panels:* The ratio $\sigma_{\rm abs}/\sigma_{\rm obs}$ corresponding to the upper panels.

on the 21cm forest (e.g. Carilli, Gnedin & Owen 2002; Mack & Wyithe 2012; Ciardi et al. 2013), the intrinsic radio source spectrum, $S_{\rm in}$, is assumed to be similar to Cygnus A, with a power-law with index $\alpha = 1.05$ and a flux density $J = 50$ mJy and 10 mJy. The simulated absorption spectrum, $S_{\rm abs}$, is calculated from the simulations mentioned above. The observed spectrum, $S_{\rm obs}$, is calculated assuming an observation time $t_{\rm int} = 1000$ h with the LOFAR and SKA1-low telescopes and a bandwidth $\Delta\nu = 10$ kHz. A clear absorption signal is observed. This is more evident in the lower panels of Figure 1, which show the quantity $\sigma_{\rm abs}/\sigma_{\rm obs}$, where $\sigma_i = S_i - S_{\rm in}$ and $i$=abs, obs. As already mentioned above, the inclusion of Ly-$\alpha$ or x-ray heating could suppress or reduce the absoprtion features, with the extent of the effect being highly dependent on the source model (see e.g. Mack & Wyithe 2012; Ciardi et al. 2013).

Very strong absorption features could be easily detected also at lower redshift, when most of the IGM is in a high ionization state, if we were lucky enough to intercept high density cold pockets of gas (with $\tau_{21\rm cm} > 0.1$; these cells are found in $\sim 0.1\%$ of the LOS in the simulation), as shown in Figure 2.

Moving towards higher redshift, when most of the gas in the IGM is still neutral and relatively cold, would offer the chance of detecting a stronger average absorption (rather than the single absorption features observed at lower redshift). If a radio source with characteristics similar to the ones described above were found, SKA1-low would easily detect the global absorption as shown in Figure 3, although it would not be straightforward to distinguish whether the suppression of the

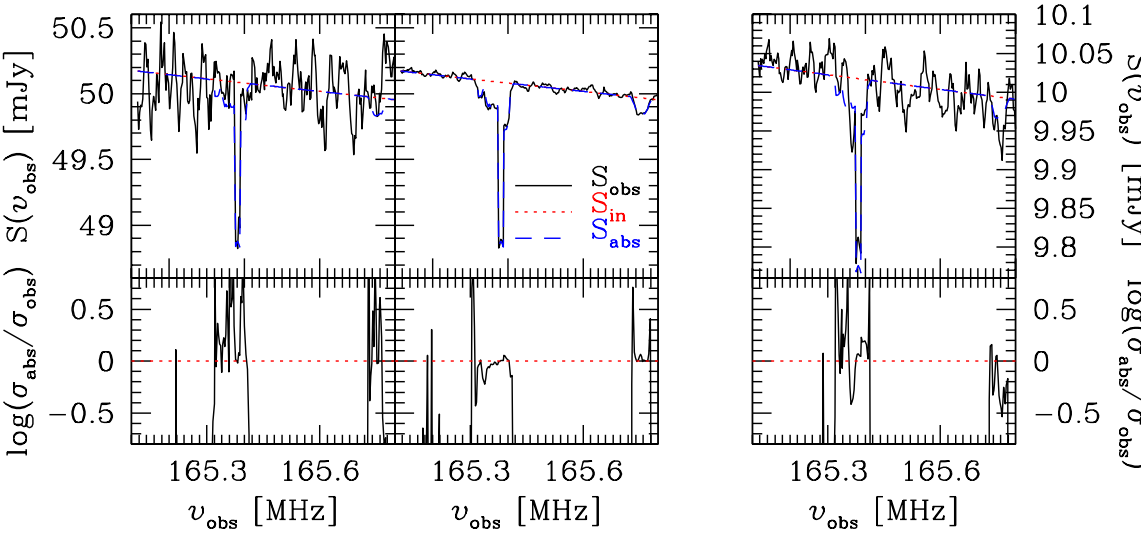


**Figure 2:** *Upper panels:* Spectrum of a radio source positioned at $z = 7.6$ ($\nu \sim 165$ MHz), with a power-law index $\alpha = 1.05$ and a flux density $J = 50$ mJy (left hand panels) and 10 mJy (right hand panel). The red dotted lines refer to the instrinsic spectrum of the radio source, $S_{\rm in}$; the blue dashed lines to the simulated spectrum for 21cm absorption, $S_{\rm abs}$ (in a universe where neutral regions remain cold); and the black solid lines to the spectrum for 21cm absorption as it would be seen with an observation time $t_{\rm int} = 1000$ h and a frequency resolution $\Delta\nu = 5$ kHz. The first panel to the left corresponds to a case with the LOFAR noise, while the other two panels have 1/10th of the LOFAR noise, roughly expected for SKA1-low. *Lower panels:* The ratio $\sigma_{\rm abs}/\sigma_{\rm obs}$ corresponding to the upper panels.

source flux were due to the intervining neutral IGM or an intrinsically lower flux.

## 3. Challenges

The most challenging aspect of the detection of a 21cm forest remains the existence of high-$z$ radio loud sources. Although a QSO has been detected at $z = 7.085$ (Mortlock et al. 2011), it is radio quiet (Momjian et al. 2014), and the existence of even higher redshift quasars is uncertain. To observe the absorption features in the spectrum, this has to be observed with a certain precision, which depends on the brightness of the quasar and the sensitivity of the instruments. The minimum detectable flux density of an interferometer can be written as:

$$\Delta S_{\rm min} = \frac{2\,\kappa_B\,T_{\rm sys}}{A\sqrt{\Delta\nu\,t_{int}}}\frac{S}{N}, \tag{3.1}$$

where $A$ is the collecting area of the array and $S/N$ is the signal-to-noise ratio. As one may not be able to distinguish whether the flux decrement were due to the diffuse IGM or an intrinsically lower flux, we will probably only detect the additional absorptions with respect to the absorption by the IGM. Therefore, the minimum flux density of the background source required to observe the absorption lines is:

$$S_{\rm min} = 10.3{\rm mJy}\left(\frac{S/N}{5}\right)\left(\frac{0.01}{e^{-\tau_{\rm IGM}}-e^{-\tau}}\right)\left(\frac{5{\rm kHz}}{\Delta\nu}\right)^{1/2}\left(\frac{1000\,{\rm m^2K^{-1}}}{A/T_{\rm sys}}\right)\left(\frac{1000\,{\rm hr}}{t_{\rm int}}\right)^{1/2}. \tag{3.2}$$

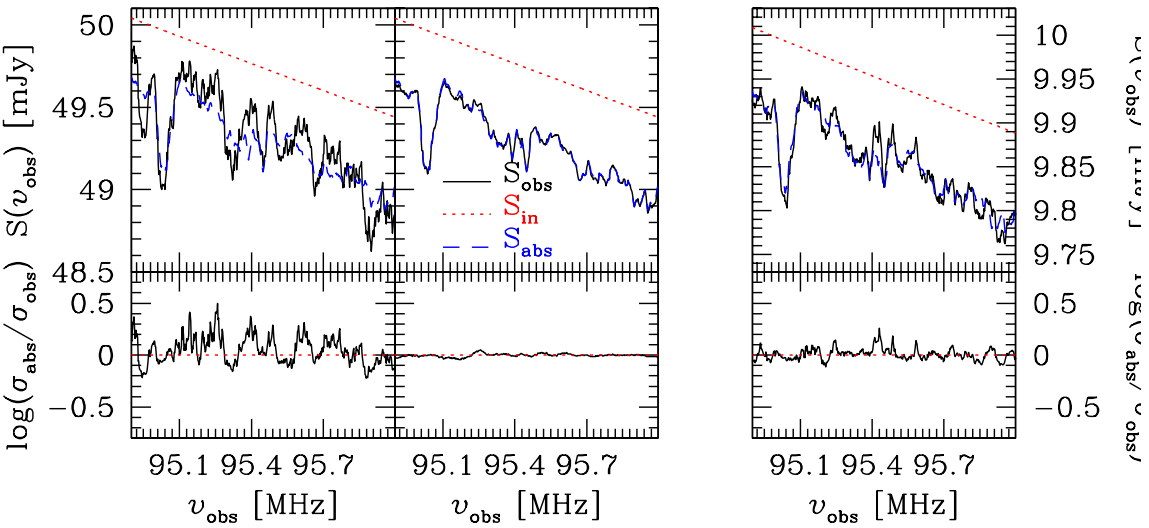


**Figure 3:** *Upper panels:* Spectrum of a radio source positioned at $z = 14$ ($\nu \sim 95$ MHz), with a power-law index $\alpha = 1.05$ and a flux density $J = 50$ mJy (left hand panels) and 10 mJy (right hand panel). The red dotted lines refer to the instrinsic spectrum of the radio source, $S_{\rm in}$; the blue dashed lines to the simulated spectrum for 21cm absorption, $S_{\rm abs}$ (in a universe where neutral regions remain cold); and the black solid lines to the spectrum for 21cm absorption as it would be seen with an observation time $t_{\rm int} = 1000$ h and a frequency resolution $\Delta\nu = 20$ kHz. The first panel to the left corresponds to a case with the LOFAR noise, while the other two panels have 1/10th of the LOFAR noise, roughly expected for SKA1-low. *Lower panels:* The ratio $\sigma_{\rm abs}/\sigma_{\rm obs}$ corresponding to the upper panels.

The SKA1-low will have $A/T_{\rm sys} \sim 1000{\rm m}^2{\rm K}^{-1}$, and we expect $A/T_{\rm sys} \sim 4000{\rm m}^2{\rm K}^{-1}$ for SKA2-low.

Extrapolating the observed number density of radio sources at $z = 4$ (Jarvis et al. 2001) to higher redshift and lower luminosity, one can calculate the number of quasars with flux density at the observed frequency $\nu_{obs} = 1420.4/(1+z)$ MHz larger than the lower limit described above, for a flat evolution model and a steep evolution model respectively (Xu et al. 2009). Using the planned SKA sensitivities, the predicted numbers of qualified radio sources are plotted in Fig.4.

The predicted number of radio sources which can be used for 21cm forest studies in the whole sky per unit redshift at $z = 10$ varies in the range $8 \times 10^2 - 2 \times 10^4$. This expected number, which is based on observations at redshift lower than reionization, is very uncertain. The exact number depends on the model adopted for the luminosity function of such sources and the instrumental characteristics (e.g. Carilli, Gnedin & Owen 2002; Xu et al. 2009), making such a detection an extremely challenging task. As a reference, the estimated quasar number per unit redshift at $z = 10$ for the 3-tiered survey is reported in Table 1.

If a sufficiently bright radio loud quasar were found beyond the redshift of reionization, then the absorption lines generated from early non-linear structures could be easily detected, as the spectral resolution of the SKA will not be a problem. Assuming the minimum halo mass hosting cold neutral gas to be $10^6{\rm M}_\odot$, about one absorption line in every 8.4kHz is expected at redshift $z \sim 10$. The absorption line density is lower for lower redshift and higher minimum mass. On

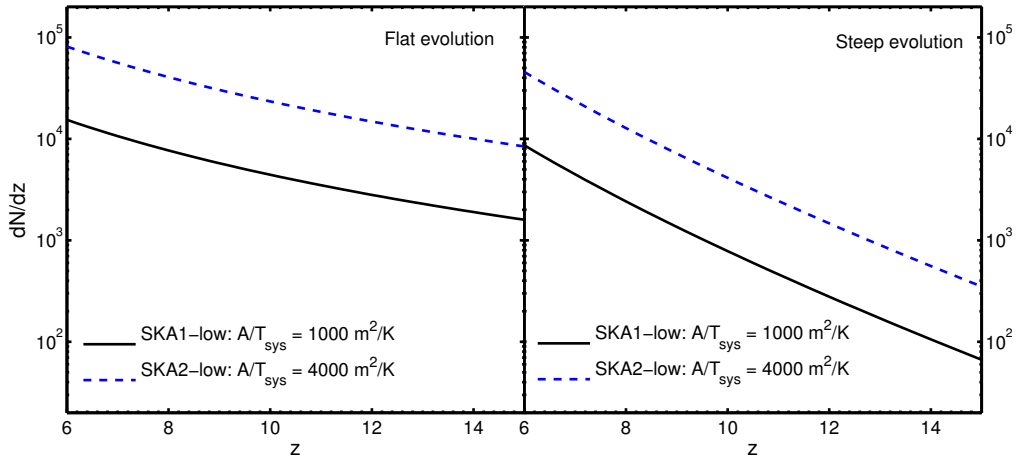


**Figure 4:** The number of quasars in the whole sky that can be used to detect signals with $e^{-\tau_{\rm IGM}} - e^{-\tau} \geq 0.01$ per redshift interval. The sensitivity of the radio array is taken to be $A/T_{\rm sys} = 1000$ m$^2$K$^{-1}$ (black solid lines) and 4000 m$^2$K$^{-1}$ (blue dashed). The integration time is assumed to be 1000 hours. *Left panel*: the number of qualified quasars in the flat evolution model. *Right panel*: the number of qualified quasars in the steep evolution model.

| $dN/dz$ | Model | $\Omega$ [sqd] | $t_{\rm int}$ [h] | $A/T_{\rm sys}$ [m$^2$K$^{-1}$] |
|---|---|---|---|---|
| 11 | Flat | 100 | 1000 | 1000 |
| 27 | Flat | 1000 | 100 | 1000 |
| 68 | Flat | 10000 | 10 | 1000 |
| 57 | Flat | 100 | 1000 | 4000 |
| 142 | Flat | 1000 | 100 | 4000 |
| 358 | Flat | 10000 | 10 | 4000 |
| 2 | Steep | 100 | 1000 | 1000 |
| 5 | Steep | 1000 | 100 | 1000 |
| 12 | Steep | 10000 | 10 | 1000 |
| 10 | Steep | 100 | 1000 | 4000 |
| 25 | Steep | 1000 | 100 | 4000 |
| 63 | Steep | 10000 | 10 | 4000 |

**Table 1:** Estimated quasar number at $z = 10$ for the 3-tiered survey. The columns refer to: number per unit redshift, source model, survey area, observation time, $A/T_{\rm sys}$.

the other hand, the line width from non-linear structures ranges mostly from $\sim$ 1kHz to $\sim$ 5kHz. Given that the SKA1-low will have a spectral resolution of 1kHz, the line counting is feasible as long as sufficiently bright radio sources are available at high redshift. Especially, if one stacks together several lines to get an average profile, it will hopefully reveal the physical status of the early non-linear structures.

An alternative possibility is the radio afterglows of certain types of gamma-ray bursts (GRBs). GRBs have already been observed up to $z \sim 8-9$, and it is plausible that they occur up to the earliest epochs of star formation in the universe at $z \sim 20$ or higher. In addition, they have a simple power-law spectrum at low frequencies, making the signal extraction easy. However, if such GRBs are similar to those seen at lower redshifts, their radio afterglows are not expected to be bright enough at the relevant observed frequencies $\nu_{\rm obs} \lesssim 100$ MHz due to strong synchrotron self-absorption (Ioka & Meszaros 2005; Inoue, Omukai & Ciardi 2007). On the other hand, it has been recently proposed that GRBs arising from Population (Pop) III stars forming in metal-free or very metal poor environments may be much more energetic compared to ordinary GRBs, leading to blastwaves expanding to much larger radii, and consequently much brighter low-frequency radio afterglows, exceeding tens of mJy (Toma, Sakamoto & Mészáros 2011). This occurs over timescales of up to $\sim$ 1000 yr, making them virtually steady radio sources, differently from more standard, lower redshift GRBs which, on the other hand, offer relatively short integration times and a limited spectral length between the location of the GRB and the end of reionization (e.g. Xu et al. 2011). In Figure 5 we show an example of absorption spectra in high-$z$ GRBs, from both Pop III and Pop II stars (Ciardi et al., in prep).

If the rate of Pop III GRBs with sufficiently bright radio emission is 0.1 yr$^{-1}$ or roughly $10^{-4}$ of all GRBs, one may expect $\sim$ 100 such sources all sky at a given time. A practical question that remains is how we can observationally identify such sources. One possibility of using GRB afterglows as the background radio source is the broad-band observation, measuring the mean flux decrement in each band without resolving individual absorption lines (Xu et al. 2011).

## 4. Discussion and Summary

As explained above, absorption features due to small collapsed objects can be much stronger than those due to the diffuse neutral IGM. Since their cross-sections are small, the best conditions for detecting them would be when Ly-$\alpha$ coupling pushes the spin temperature in their lower density outskirts to the gas temperature before these regions have been affected by any heating (see Fig. 22 in Meiksin 2011), conditions expected above $z \sim 10$. However, even after heating has started to suppress the 21cm absorption signal, some weak features due to collapsed structures may remain. Interestingly, even when it may not be possible to detect these weak features individually, the presence of absorption may be detected statistically. Weak absorption would produce an increase in the variance of brightness fluctuations, as an addition to the telescope noise, resulting in an apparently noisier spectrum blue-ward of the 21cm transition (see Fig. 29 in Meiksin 2011; Fig. 8 in Mack & Wyithe 2012). The possibility to have a statistical detection of the 21cm forest (rather than the detection of single absorption features), is intriguing as the signature of the forest would be observed in the 21cm power spectrum (see also Ewall-Wice et al. 2013). By integrating the signal from many high redshift sources within the field of view, would reduce the sensitivity requirements

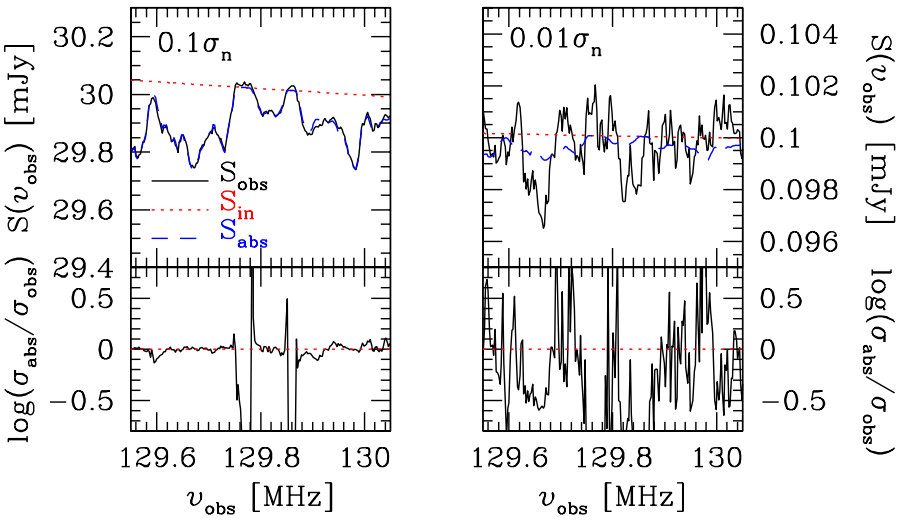


**Figure 5:** *Upper panels:* Spectrum of a GRB positioned at $z = 10$ ($\nu \sim 129$ MHz), with a power-law index $\alpha = 0.5$ and a flux density $J = 30$ mJy (GRB from Pop III stars; left hand panel) and 0.1 mJy (GRB from Pop II stars; right hand panel). The red dotted lines refer to the instrinsic spectrum of the source, $S_{\rm in}$; the blue dashed lines to the simulated spectrum for 21cm absorption, $S_{\rm abs}$ (in a universe where neutral regions remain cold); and the black solid lines to the spectrum for 21cm absorption as it would be seen with an observation time $t_{\rm int} = 1000$ h and a frequency resolution $\Delta\nu = 10$ kHz. The panel to the left (right) corresponds to a case with 1/10th (1/100th) of the LOFAR noise, roughly expected for SKA1-low (SKA2-low). *Lower panels:* The ratio $\sigma_{\rm abs}/\sigma_{\rm obs}$ corresponding to the upper panels.

of the instrument. On the other hand, the main problem of the paucity of high-$z$ radio sources would persist.

The attempt to detect the 21cm forest has the potential to provide unprecedented information about the large-scale evolution of the intergalactic medium as well as the growth of small-scale structures. Different information can be gleaned depending on the nature of the observation. An attempt to detect the presence of the 21cm forest via a statistical analysis of the power spectrum (Ewall-Wice et al. 2013) will allow us to put constraints on the presence of high-redshift radio-loud sources at high wavenumbers ($k \gtrsim 0.5$ Mpc$^{-1}$), and to study the IGM thermal history at low wavenumbers ($k \lesssim 0.1$ Mpc$^{-1}$). Assuming high-redshift radio-loud sources are identified, and we are able to observe them directly in targeted observations, detailed study of the source spectra can reveal the mean thermal properties of the IGM via the flux decrement (Furlanetto 2006) or variance in the flux (Carilli et al. 2004; Mack & Wyithe 2012). If individual absorption features are identified in the spectrum, this could allow us to put constraints on the clumping factor at early times (Xu, Ferrarra & Chen 2011) and to map structure along the line of sight (IGM and/or the first collapsed structures and mini-halos), thus significantly extending our understanding of the process of reionization and the hierarchical growth of structure in the Universe.

Finally, we would like to comment on the fact that as observations of the 21 cm forest require very high frequency resolution, they are demanding both in terms of data storage and processing. However, when a bright continuum radio source is identified after an all-sky survey or deep EoR

observations, it is possible to significantly average in time after phasing up to the source. The maximum amount of data compression will be dictated by the need to identify and subtract bright, far away sources that may generate sidelobe noise in the measurement of the 21 cm forest. However, if bright sources are measured a priori from a sky survey they can be subtracted from the high time resolution visibilities and, afterwards, data can be easily compressed by an order of magnitude or more.

## References

Carilli, C. L., Wang, R., van Hoven, M. B., et al. 2007, AJ, 133, 2841
Carilli, C. L., Gnedin, N. Y., Owen, F. 2002, ApJ, 577, 22
Ciardi, B., Bolton, J. S., Maselli, A., Graziani, L. 2012, MNRAS, 423, 558
Ciardi, B. et al. 2013, MNRAS, 428, 1755
Ciardi, B., Ferrara, A. 2005, Space Science Reviews, 116, 625
Ewall-Wice, A., Dillon, J. S., Mesinger, A., Hewitt, J. 2014, arXiv:1310.7936
Furlanetto, S. R. 2006, MNRAS, 370, 1867
Furlanetto, S. R., Oh, S. P., Briggs, F. H. 2006, Phys. Rep., 433, 181
Furlanetto, S. R., Loeb, A. 2002, ApJ, 579, 1
Inoue, S., Omukai, K., Ciardi, B. 2007, MNRAS, 380, 1715
Ioka, K., Mészáros, P. 2005, ApJ, 619, 684
Jarvis, M. J., Rawlings, S., Willott, C. J., et al. 2001, MNRAS, 327, 907
Mack, K. J., Wyithe, J. S. B. 2012, MNRAS, 425, 2988
Madau, P., Meiksin, A., Rees, M. J. 1997, ApJ, 475, 429
Meiksin, A. 2011, MNRAS, 417, 1480
Momjian, E., Carilli, C. L., Walter, F., Venemans, B. 2014, arXiv:1310.7960
Mortlock, D. J., et al. 2011, Nature, 2011, 1106
Shimabukuro, H., Ichiki, K., Inoue, S., Yokoyama, S. 2014, arXiv:1403.1605
Toma, K., Sakamoto, T., Mészáros, P. 2011, ApJ, 731, 127
Xu, Y., Chen, X., Fan, Z.,Trac, H., Cen, R. 2009, ApJ, 704, 1396
Xu, Y., Ferrara, A., Chen, X. 2011, MNRAS, 410, 2025